BIOCHEMICAL PHARMACOLOGY 72 (2006) 1405–1416

available at www.sciencedirect.com

ScienceDirect

journal homepage: www.elsevier.com/locate/biochempharm

Different fates of intracellular glutathione determine different modalities of apoptotic nuclear vesiculation

Milena De Nicola [a], *Giampiero Gualandi* [c], *Alberto Alfonsi* [c], *Claudia Cerella* [a], *Maria D'Alessio* [a], *Antonio Bergamaschi* [d], *Andrea Magrini* [b], *Lina Ghibelli* [a,*]

[a] *Dipartimento di Biologia, Universita' di Roma Tor Vergata, via Ricerca Scientifica, 100133 Roma, Italy*
[b] *Cattedra Medicina del Lavoro, Universita' di Roma Tor Vergata, Italy*
[c] *DABAC, Universita' della Tuscia, Viterbo, Italy*
[d] *Cattedra Medicina del Lavoro, Universita' Cattolica Sacro Cuore, Roma, Italy*

ARTICLE INFO

Article history:
Received 28 April 2006
Accepted 9 June 2006

Keywords:
Apoptosis
Nuclear morphologies
Budding
Cleavage
In situ glutathione measurement
Epstein Barr Virus

ABSTRACT

U937 monocytic cells show two main apoptotic nuclear morphologies, budding and cleavage, that are the result of two independent morphological routes, since they never interconvert one into the other, and are differently modulated by stressing or physiological apoptogenic agents [Exp Cell Res 1996; 223:340–347]. With the aim of understanding which biochemical alterations are at the basis of these alternative apoptotic morphologies, we performed an *in situ* analysis that showed that in U937 cells intracellular glutathione (GSH) is lost in cells undergoing apoptosis by cleavage, whereas it is maintained in apoptotic budding cells. Lymphoma cells BL41 lose GSH in apoptosis, and show the cleavage nuclear morphology; the same cells latently infected with Epstein Barr Virus (E2r line) undergo apoptosis without GSH depletion and show the budding nuclear morphology. GSH depletion is not only concomitant to, but is the determinant of the cleavage route, since the inhibition of apoptotic GSH efflux with cystathionine or methionine shifts the apoptotic morphology from cleavage to budding. Accordingly, cystathionine or methionine antagonizes apoptosis in the all-cleavage BL41, without affecting the all-budding E2r.

1. Introduction

Apoptosis is the result of the coordinated involution of cellular structures, achieved through multiple independent pathways whose choice depends on cell type and/or apoptotic stimulus, i.e., physiological versus cell-damaging. The two pathways evolve through independent set of events [1], carried on by protein–protein interactions and conformational changes, culminating in the assembly of different protein complexes, DISC or apoptosome, which recruit and activate the upstream caspases (8 or 9, respectively), which in turn activate caspase 3; this pivotal caspase coordinate the activation of the executioner caspases contributing to execute and orchestrate the morpho-functional cellular involution [2–6]. The convergence of both apoptotic pathways into the activation of caspase 3, implies that they share the execution phase and would suggest that the final morphological/biochemical features of apoptotic cells are the same, independently of the apoptogenic stimulus.

The knowledge of different signal pathways, allows re-evaluating previous apparently contradictory results concerning the events occurring during apoptosis, and their respective roles. In particular, this applies to the role of oxidative stress and redox imbalance in the signal transduction events of apoptosis. It now appears that oxidative alterations are absent, or at least

* *Corresponding author*. Tel.: +39 06 7259 4323; fax: +39 06 2023500.
E-mail address: ghibelli@uniroma2.it (L. Ghibelli).
0006-2952/$ – see front matter
doi:10.1016/j.bcp.2006.06.009

unnecessary, for the development of the physiological pathway, being instead required for the damage-induced mitochondrial pathway [7]. Apoptosing cells get rid of reduced glutathione prior to apoptosis [8] by promoting its efflux via specific carriers: this is a *sine qua non* for damage-induced apoptosis [9], but only circumstantial [10], or even absent [11], for receptor-mediated apoptosis. It has been shown that the depletion of glutathione is necessary and sufficient to induce cytochrome c release [12], promoting Bax dimerization and translocation to mitochondria [11]. It is conceivable that the redox unbalance that characterizes the mitochondrial pathway, exerts some effects on additional redox sensitive cellular targets, which in turn may affect the final stages of apoptosis. Many redox sensitive targets have been shown to be involved in apoptosis, such as caspases [13] glyceraldehyde3phosphatedehydrogenase [14], glutathione-S-transferase [15]; multiprotein complexes performing functions involved in apoptosis, such as Ca^{2+} channel, are regulated by disulfide formation [16]. The assembly and remodelling of actin cytoskeleton is regulated by, and very sensitive to, redox alterations [17], and is involved in the deep morphological alterations occurring in apoptosis known as cytoplasmic blebbing [18].

The change of nuclear shape is one of the most prominent morphological alterations in apoptosis, often used as a diagnostic of apoptosis both in anatomic tissue sections and cell cultures. It may consist of a deep shrinkage, possibly due to deregulation of ion pumps plus loss of nuclear pore functions. Alternatively, nuclei dissolve into a number of vesicles, through regulated processes depending on cytoskeletal rearrangements such as nuclear lamin breakdown and actin reorganization, perhaps recalling nuclear shaping occurring under physiological conditions, i.e., maturation of polymorphonuclear neutrophils.

In a TEM study we had previously described multiple pathways for apoptotic nuclear vesiculation, occurring in U937 cells as a response to different apoptogenic agents; the identification of intermediate stages allowed us to demonstrate that the different morphologies do not interconvert one into the other, but are the result of independent pathways [19]. The main discriminant is the type of nuclear vesiculation, occurring by hypercondensation of metaphase chromosomes in mitotic cells; in interphase cells by budding of nuclear vesicles (''budding'' type), or by cleavage of the nuclear sap (''cleavage'' type). For interphase cells, being the predominant ones, the choice between the budding or the cleavage route depends mainly on the type of inducer [19]. Even though it seems reasonable to attribute the different morphological features to different biochemical reactions, the mechanisms at the basis of the choice between the cleavage and the budding mode of apoptotic nuclear vesiculation are not known. The *in situ* analysis of several biochemical parameters associated to the two apoptotic morphologies reveal that cells undergoing budding or cleavage differ in many respects, but share the ''canonical'' apoptotic features such as loss of mitochondrial transmembrane potential, DNA laddering and caspase 3 activation, thus being frankly apoptotic (De Nicola et al., in preparation).

With the aim of exploring such biochemical differences, in this study we investigate whether the two morphologies may reflect a different redox status of the apoptosing cells. We found that, in three cell lines, GSH depletion is associated to, and responsible for, the events leading to the cleavage nuclear morphology.

2. Materials and methods

2.1. Cell culture and treatments

2.1.1. Cell culture

U937 are human pro-monocytes derived from a istiocytic lymphoma; BL41 are from a Burkitt, Epstein-Barr Virus (EBV) negative B cell lymphoma. E2r were obtained by in vitro infection of BL41 with the B95-8 strain of EBV, and subsequent cloning [20]. All cells were cultured in RPMI 1640 medium supplemented with 10% FCS, 2 mM L-glutamine, 100 IU/ml penicillin and streptomycin, and kept in a controlled atmosphere (5% CO_2) incubated at 37 °C. The experiments were performed on cells in the logaritmic phase of growth, in conditions of excellent viability, as assessed by trypan blue exclusion, $\geq$98%.

2.1.2. Induction of apoptosis

Apoptosis was induced with the protein synthesis inhibitor puromycin (SIGMA, PMC, 10 ug/ml for U937 and 3 ug/ml for BL41 and E2r) or with the topoisomerase II inhibitor etoposide (VP16, 100 ug/ml). All compounds were kept throughout the experiment.

2.1.3. Analysis of apoptosis

For detection of apoptosis, cells were stained with the DNA-specific, cell permeant dye Hoechst 33342 (Calbiochem) at the concentration of 10 ug/ml, without prior fixation; apoptotic cells were recognized according to their nuclear morphology (different stages of nuclear fragmentation) [19,21]. Propidium iodide (10 ug/ml) was added for detection of eventual cells in secondary necrosis.

2.1.4. Quantification of apoptosis

Apoptosis was quantified as previously described [9]. Briefly, the fraction of U937 or BL41 or E2r cells with fragmented nuclei among the total cell population is calculated in the Hoechst 33342 stained cells, counting at least 300 cells in at least 10 random selected fields.

2.1.5. Inhibition of GSH efflux

Cells were treated with 1 mM cystathionine or 1 mM methionine; the compounds were added 1 h before the apoptogenic treatment and kept throughout the experiment.

2.2. Fluorescence measurements

2.2.1. Analysis of GSH content

The *in situ* analysis of GSH was carried out with the use of three different permeant fluorescent GSH probes: 5-chloromethylfluorescein diacetate (CMFDA); monochlorobimane (MCB); o-phthaldehyde (OPTA). The probes have different features and different mechanisms of action. CMFDA is excitable by the 488 laser line, has green emission and requires glutathione S-transferase (GST) to form a fluorescent conjugate, potentially conferring specificity for GSH. MCB as well requires the

presence of GST, however, it has a UV excitation and blue emission. Conversely, OPTA does not require GST for adduct formation with GSH, it is excited by the UV lamp and has a blue emission. CMFDA and MCB were purchased from Molecular Probes, OPTA was purchased from Sigma.

Cultures were prepared for fluorescence measurements by washing and resuspending in RPMI without phenol red. Cultures were incubated at 37 °C with 10 nM (U937) or 20 nM (BL41 and E2r) CMFDA for 15 min; or with 50 uM MCB or 50 uM OPTA for 20 min. Treated and untreated samples were stained under identical conditions.

2.2.2. *Analysis of mitochondrial transmembrane potential (mtΔΨ)*

Cells were loaded with 100 nM mitoTracker red (Molecular Probes) by incubating at 37 °C for 10 min. Cells were then immediately analysed by flow cytometry.

2.2.3. *Flow cytometric measurements*

All the flow cytometric measurements were performed with a Galaxy Flow cytometer (Partec FloMax 2.0), which is equipped with a mercury high pressure lamp and a 488 laser. This particular configuration allowed us the possibility to use probes with different excitation wave lengths (lamp and laser) together with the forward and side scatter information (laser). Each flow cytometric measurements was carried out on at least 20000 cells.

2.2.4. *Fluorescence microscopy and digital photomicrography*

For fluorescence microscopy analysis stained cells were observed at the fluorescence microscopy with a Nikon Eclipse TE 200 microscope equipped with a 100 W mercury lamp. Images were recorded with a CoolSNAP digital camera. The microscopic fields shown are reconstituted starting from different fields in the same microscopic slide, using an on purpose grid to assure fidelity in the reconstitution. Adjustments of contrast or brightness, performed in order to maximise picture quality, were applied only after reconstitution of the fields.

2.2.5. *Quantitative image analysis*

The extent of CMFDA fluorescence of BL41 and E2r cells was elaborated with NIH Image 1.61 programme. Area, mean fluorescence and fluorescence with respect to background was calculated for each cell. Single cell fluorescence was calculated as follows: (mean fluorescence − background fluorescence) × area.

2.2.6. *Statistical analysis*

Statistical analyses were performed using Student's *t*-test for unpaired data and p values < 0.05 were considered significant. Data are presented as mean ± S.D.

3. Results

3.1. *In situ analysis with three different GSH intracellular probes on apoptosing U937 cells*

The analysis of GSH in apoptosis at the single cell level requires an *in situ* analysis. Thus, we decided to switch from the standard HPLC analysis [9] to an *in situ* methodology with fluorescent probes. Several cell-permeant fluorescent probes for GSH are available; we chose three of them, that work in different ways: 5-chloromethylfluorescinediacetate (CMFDA) [22], and monochlorobimane (MCB) [23,24], that fluoresce when complexed with GSH by glutathione-*S*-transferase; *o*-phtaldehyde (OPTA) [24,25], that fluoresces upon reaction with small thiols. Their ability to detect intracellular variations of GSH was probed at the flow cytometer by increasing GSH concentration with *N*-acetyl-cysteine (10 mM for 24 h; all three probes were sensitive, not shown), or by decreasing it with buthionine sulphoximine (1 mM for 24 h; OPTA and MCB were sensitive, whereas CMFDA was not; not shown).

Apoptosis was induced with 10 ug/ml PMC; untreated cells and cells at 2.5 h of treatment with PMC, were stained with CMFDA, MCB or OPTA, and analysed at the flow cytometer. Fig. 1A shows that untreated cells form a quite homogeneous population in terms of stainability with any of the three probes. Instead, in treated samples a new population of cells with reduced fluorescence appears, while the main peak maintained a level of fluorescence similar to controls. Similar results are obtained with the three probes, thus excluding that this is due to some idiosyncrasies of the single probes. Since no loss of protein thiols is detected in apoptotic U937 cells (as detected by thiol derivatization of cell lysates protein fractions, data not shown), the low-fluorescence peak indicates cells that have lost GSH. The loss is likely to be very rapid, since the extra peak is clearly separated by the main peak, indicating a yes-or-no situation.

The quantification of the peak areas reveals that the ratio of cells positioned in the low versus high fluorescence peaks is similar for all the three probes used (i.e., the probes see the same thing), and the values are quite close to those found by measuring total GSH content by HPLC (not shown). Similar results were obtained with VP16 (not shown).

When we compare the fraction of low fluorescent cells with the fraction of cells with the nuclear features of apoptosis (see Fig. 1B), we observe that more apoptotic cells than cells with low GSH exist. This could be due to two alternative explanations: either nuclear alterations precede GSH loss; or, alternatively, we have apoptotic cells with either low or high GSH. We are tempted to exclude the first explanation, since we have already shown that GSH extrusion precedes apoptosis in U937 and HepG2 cells [8]. Thus, we decided to probe the second one.

3.2. *Two different fates of intracellular GSH in apoptotic U937*

In order to understand whether apoptotic cells with either low or high GSH exist, we performed a flow cytometric biparametrical analysis of the time course of GSH content and apoptosis. As a marker of apoptosis we chose the loss of mitochondrial trans-membrane potential (mtΔΨ), monitored by mitotracker red (MTR). We were allowed to do so, since a comparative analysis of nuclear morphology and mtΔΨ in U937 cells revealed a perfect overlapping, i.e., all cells with low MTR stainability had an apoptotic nucleus and vice versa (not shown).

Fig. 2 shows the flow cytometric biparametric analysis of U937 cells stained with MTR and CMFDA, either untreated or induced to apoptosis by PMC for 1.5 and 2.5 h. We did not go

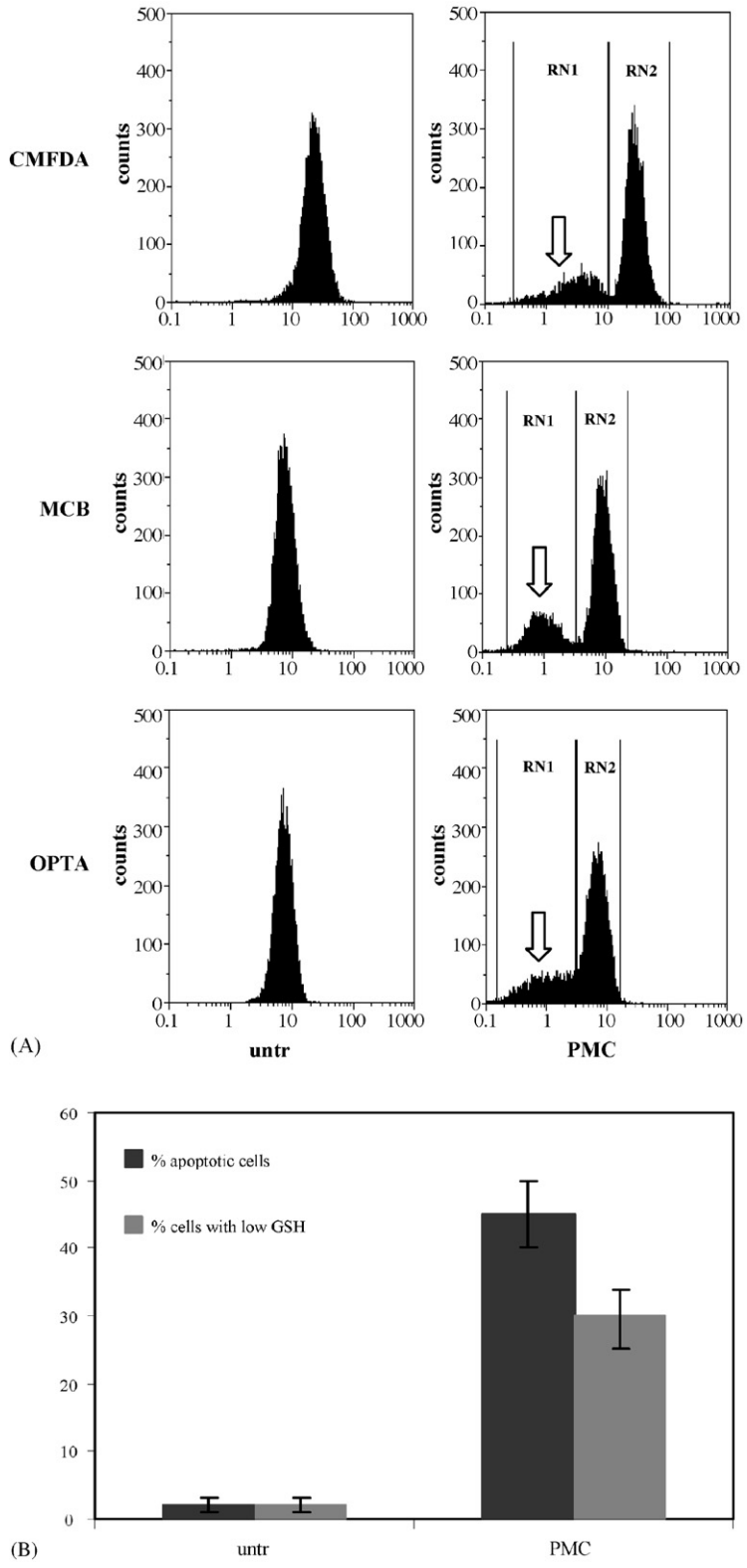

Fig. 1 – *In situ* analysis detects apoptotic GSH loss. Panel A shows the flow cytometric analysis of U937 cells, untreated and at 2.5 h of puromycin, PMC. At the end of the treatment, cells were aliquoted and stained for GSH with either CMFDA, MCB or OPTA as described in Section 2. Upon PMC (right column), a peak of weakly stained cells appears (arrow), whereas the position of the main peak is not altered. The fractions of weakly stained cells (positioned in region RN1) were similar for the three probes, being 30 ± 3%. One of four independent experiments with similar results is shown. In panel B, the average fraction of weakly stained cells (region RN1) of the four experiments for the three probes is shown (light bars) and compared with the fraction of apoptotic cells evaluated by nuclear staining (see Section 2). The fraction of apoptotic cells is significantly higher than the fraction of cells without GSH.

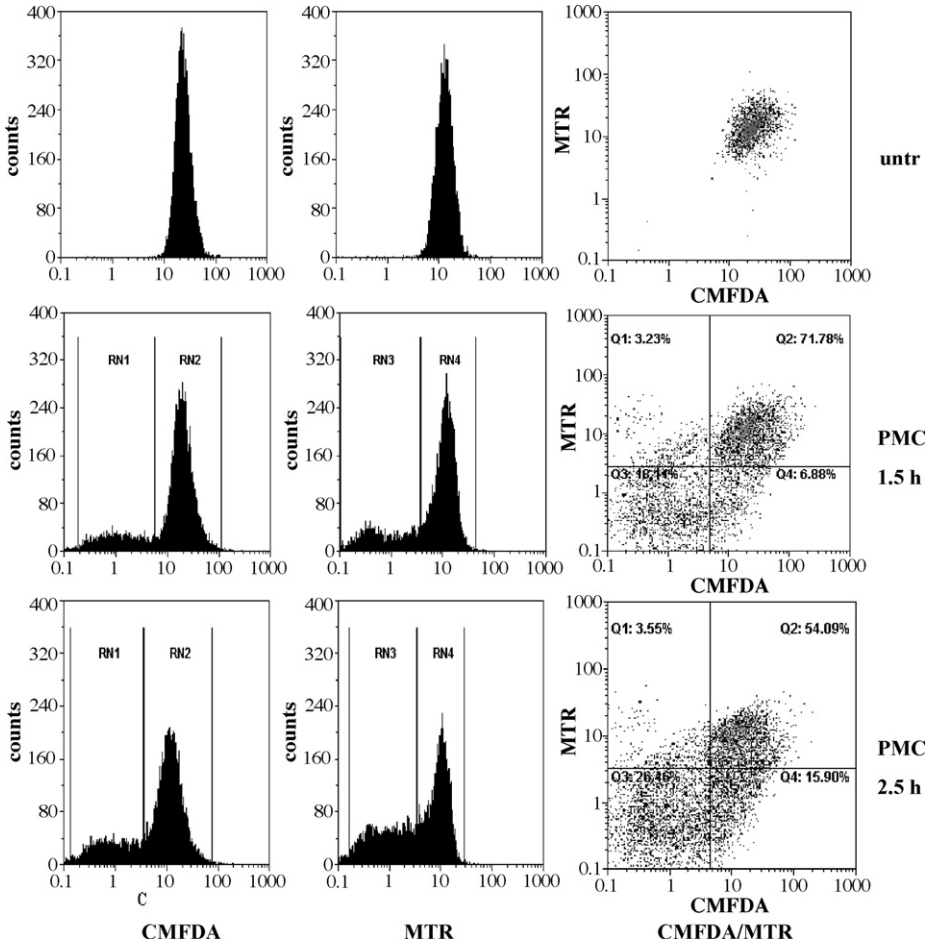

Fig. 2 – Biparametric analysis of apoptosis vs. GSH content. U937 cells were induced to apoptosis by PMC; at 1.5 and 2.5 h cells were double-stained with CMFDA (for GSH) and MTR (for apoptosis detection). Stained cells were analysed at the flow cytometer: left column shows the monoparametric GSH analysis; middle column the monoparametric analysis of apoptosis; right column the biparametric analysis of GSH vs. apoptosis. Note that the regions of low stainability with the two monoparametric analyses (RN1 and RN3, respectively) increase with time of PMC. The biparametric of CMFDA vs. MTR shows double-positive, viable cells in the upper, right quadrant (Q2), as evident in untreated cells. Instead, apoptotic cells fall in the lower, MTR-quadrants (Q3 + Q4). Apoptotic cells fall in two separate populations, with low or high GSH content (Q3 vs. Q4, respectively). Apoptotic cells with low GSH appear earlier than apoptotic cells with high GSH, suggesting that they evolve independently. Similar results were obtained in four additional experiments with double labelling with CMFDA and MTR. The results were also confirmed by two and three experiments performed with double labeling with MTR and OPTA or MCB, respectively.

any further, because at later times apoptotic cells begin to lose plasma membrane integrity (secondary necrosis), thus rendering GSH or mt$\Delta\Psi$ analysis meaningless.

Untreated cells have a homogeneous population with high CMFDA and MTR. At 1.5 h of PMC, MTR negative, i.e., apoptotic cells begin to appear. These cells are predominantly CMFDA negative, that is with low GSH content, and are positioned in quadrant Q3 (ratio CMFDA positive/negative = 0.3). At 2.5 h of PMC, the number of apoptotic cells increases, but at this time the increment is predominantly of apoptotic cells with high GSH content, i.e., positioned in quadrant Q4 (ratio CMFDA positive/negative = 0.61). The biparametric analysis of cells stained with MTR and MCB or OPTA gave the same results. These results show that apoptotic cells with low GSH appear before apoptotic cells with high GSH. Since it is quite unlikely that apoptotic cells regain GSH after its loss, we may conclude that GSH loss is not a final result of all apoptotic cells, but it is part of only one of two (or more) alternative routes.

3.3. *Different apoptotic morphologies in U937 cells in response to apoptogenic agents*

Nuclear vesiculation is one of the most dramatic and widespread features of apoptotic cells, occurring as an alternative to nuclear shrinkage. Our TEM analysis [19] showed that the two main interphase morphologies, budding and cleavage, differ in the nuclear membrane structure and the peculiar shape of chromatin clamps condensing at the border, being either a protruding, budding mass in the budding cells, or a non-protruding crescents in cells in cleavage. Nuclear

vesiculation is then completed with separation of the vesicles, by budding or by invagination and sealing of the inner and outer nuclear membrane, respectively, to reach the final fragmented morphology.

The shape of condensed chromatin is easily recognizable at the fluorescent microscopy after staining with the DNA-specific dye Hoechst 33342. In Fig. 3A we show U937 induced to apoptosis with PMC, where the different apoptotic morphologies are recognizable. The same apoptotic morphologies were observed also with VP16 (not shown).

The time course analysis of the different morphologies (budding, cleavage and fragmented) of U937 treated with PMC shows that cells in cleavage appear earlier than budding cells, both declining at later times to give rise to the final fragmented nuclei (Fig. 3B). This is reminiscent of the appearance of GSH-negative before GSH-positive apoptotic cells (see above), and suggests a possible relationship between GSH content and type of morphology.

3.4. *GSH is lost in cleavage but not in budding apoptotic U937*

In order to possibly assign apoptotic loss of GSH to one or the other type of nuclear apoptotic morphology, we performed a

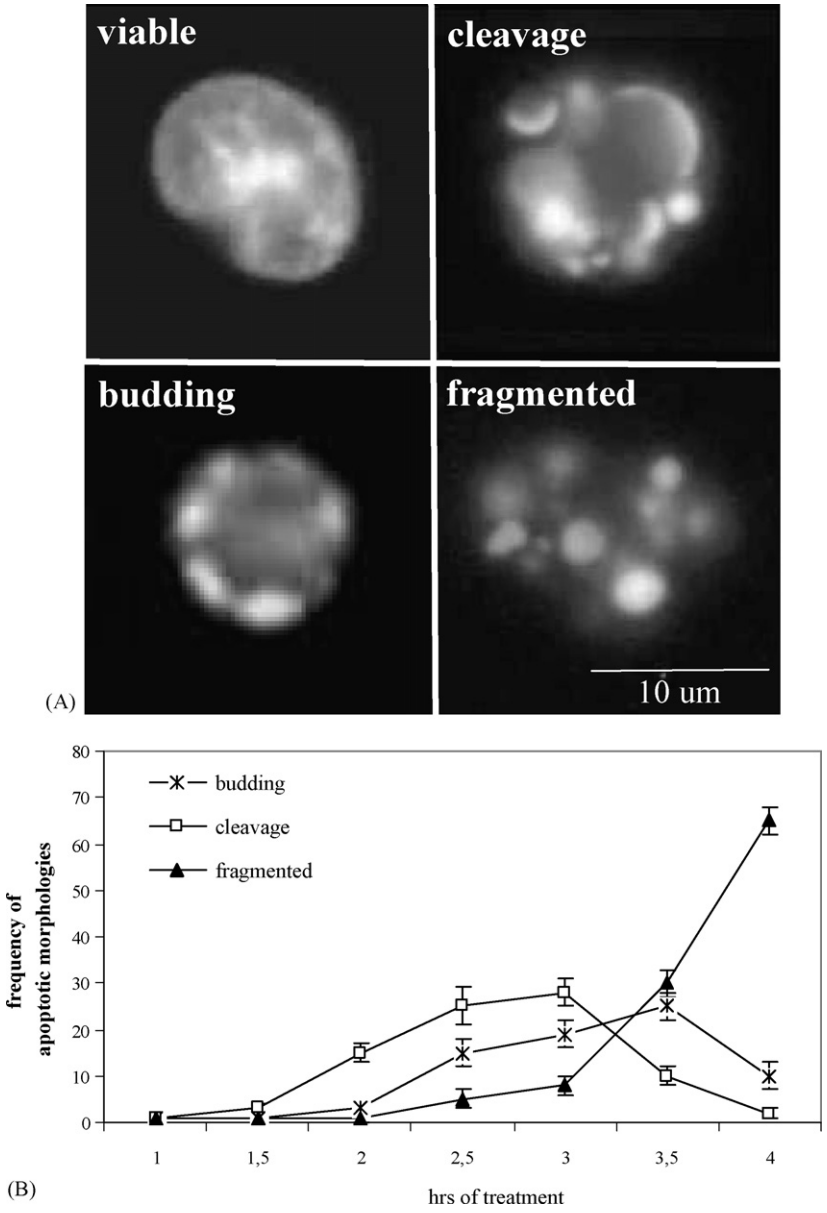

Fig. 3 – Different U937 nuclear apoptotic morphologies. Nuclear apoptotic morphology is unambiguously revealed by Hoechst 33342 staining in PMC-treated U937 cells as described in Section 2. (A) Shows the fluorescent microscopy images of nuclear morphology. Budding nucleus has protruding chromatin masses, whereas cleavage nucleus has chromatin condensed in crescent shapes. Budding and cleavage decline to give rise to the final fragmented nucleus. (B) The time course analysis of the different morphologies shows that cells in cleavage appear earlier than budding cells. Values are calculated as the average ± S.D. (n = 6). Propidium iodide (PI), included with Hoechst to label cells in secondary necrosis, showed that at 4 h about 15% of fragmented cells are PI+, whereas all cells in cleavage or budding are PI−.

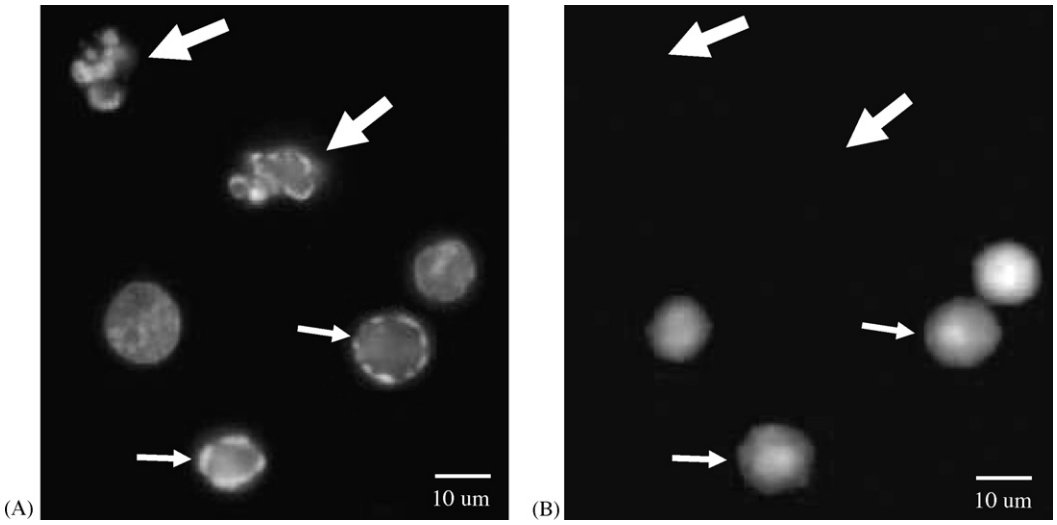

Fig. 4 – Different apoptotic morphologies correspond to different intracellular GSH content. Nuclear apoptotic morphology is unambiguously revealed by Hoechst 33342 staining in PMC-treated U937 cells as shown in panel A. Panel B shows the same field stained with CMFDA for GSH evaluation. Budding nuclei (thin arrows) maintain control level CMFDA stainability whereas cells in cleavage (thick arrows) have low GSH content. Same results were found by double labelling cells with Hoechst for nuclear morphology and MCB or OPTA for GSH (not shown), or by inducing apoptosis with VP16 (not shown).

fluorescence microscopy biparametrical analysis of cells stained with Hoechst 33342 and CMFDA. This analysis revealed a strict correlation between type of morphology and fate of GSH in apoptosis, since all budding cells (thin arrows) showed control GSH level, whereas cells in cleavage (thick arrows) had low or undetectable CMFDA stainability (Fig. 4). Similar results were obtained with VP16 (not shown).

We also analysed the CMFDA fluorescence of apoptotic cells with totally fragmented nuclei, as revealed by Hoechst staining, that are the convergence final point of both cleavage and budding cells. Cells with compromised plasma membrane, i.e., unable to exclude impermeant fluorescents such as propidium iodide (PI) were excluded because of possible artefacts. Among the PI-negative cells with fragmented nuclei, we found both CMFDA positive and negative cells, in a proportion that overlaps the proportion of clearly discernable budding versus cleavage cells (not shown). This observation suggests that ex-budding cells maintain their GSH content up to plasma membrane collapse.

3.5. *Inhibition of apoptotic GSH efflux inhibits the cleavage route*

So far, we have demonstrated the correlation between intracellular GSH content in apoptosis and type of apoptotic nuclear morphology. Now, we explore a possible cause-effect relationship between the two events. We know that apoptotic GSH extrusion occurs through the physiological synusoidal type GSH transporters, since the specific inhibitors cystathionine or methionine are able to inhibit such efflux [9]. Thus, we exploited the specific inhibitors to prove our assumption. If GSH extrusion is only associated and not responsible for the cleavage morphology, we would expect to detect, in the presence of cystathionine, cells in cleavage in spite of high GSH levels. Alternatively, if GSH extrusion is the event that determines the type of morphology, we would expect that methionine or cystathionine are able to shift the ratio between apoptotic morphologies in favour of budding. This latter alternative turned out to be correct, as results from the data in Fig. 5, that shows the fraction of each apoptotic nuclear morphology of U937 cells induced to apoptosis in the presence/absence of cystathionine or methionine. Indeed, an almost total shift towards the budding morphology is achieved by inhibition of GSH extrusion. The same experiment

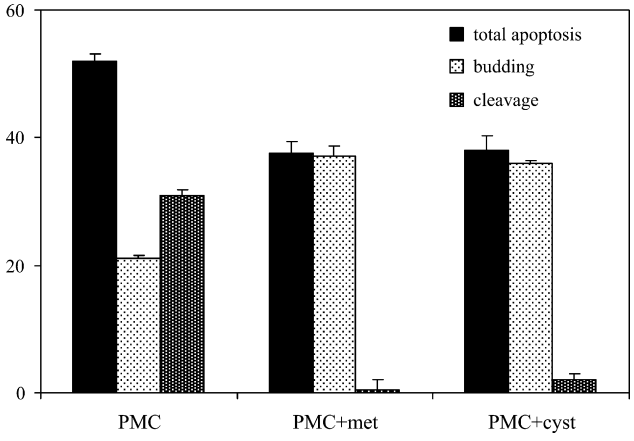

Fig. 5 – Cystathionine or methionine shift apoptotic morphology towards budding. Apoptotic morphologies were evaluated and quantified as described in Section 2 at 3 h of treatments with PMC, in the presence/absence of the inhibitors of GSH efflux cystathionine (cyst) or methionine (met). Values are calculated as the average ± S.D. (n = 5). Cystathionine or methionine by itself do not exert any apoptogenic effect (not shown). The cleavage morphology almost completely disappears following inhibition of GSH efflux.

performed with VP16, gave similar results: cystathionine and methionine induced a shift of the ratio between budding and cleavage from 58:42 to 98:2 and 99:1, respectively.

This is a key result for our study, since it places GSH extrusion as the determinant event for the cleavage morphology. Indeed, independently of what may occur upstream, it is the (rapid) loss of GSH in apoptosis that triggers the reactions leading to cleavage.

Fig. 5 also shows that cystathionine, or methionine, significantly reduce the extent of apoptosis, confirming our previous results [9]. This reduction is due to the almost complete disappearance of cells in cleavage. It is interesting to note that, in spite of the overall reduction of apoptosis, the total number of budding cells is paradoxically increased by cystathionine or methionine. Thus, inhibition of the route that leads to cleavage gives the cell two alternatives: either the apoptotic process is aborted, and the cell is rescued; or the program is somehow shifted to (or reinitiated on) the budding route.

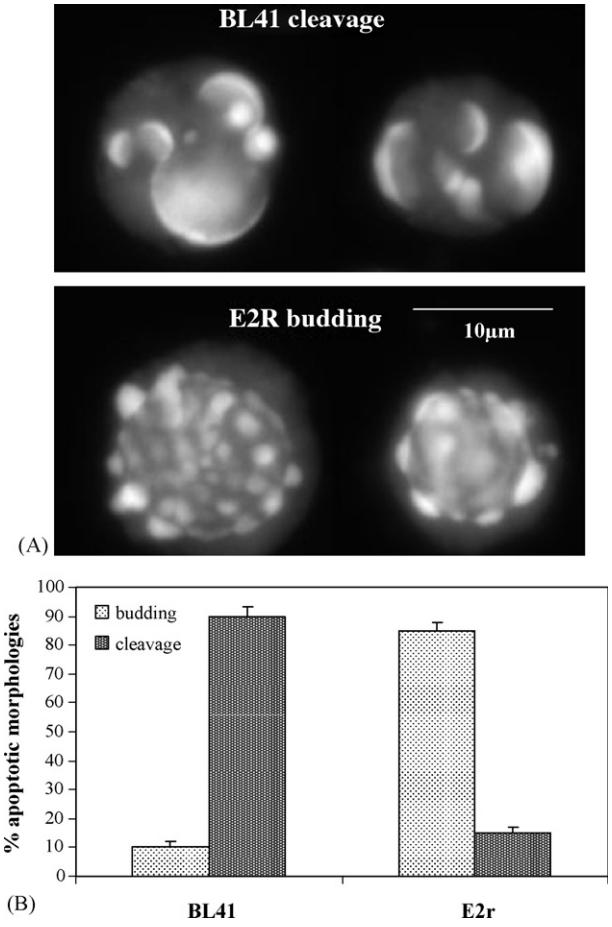

Fig. 6 – Separation of the budding and cleavage morphology in a couple of congenic lymphoma cells. BL41 Epstein Barr negative lymphoma was converted by EBV as described [25]. The parental BL41 and the converted E2r line were induced to apoptosis with PMC, stained with Hoechst 34442 and the apoptotic morphologies recorded (panel A) and quantified (panel B). The values are calculated as the fraction of each morphology for 100 apoptotic nuclei, and are the average of $n > 10$ experiments, ±S.D. The same separation of morphologies between the two cell lines was maintained with other apoptogenic inducers (not shown).

3.6. *GSH is lost in apoptosis in the all-cleavage BL41, whereas it is maintained in the all-budding E2r*

The two apoptotic nuclear morphologies are not restricted to U937 cells, but other cells of haematopoietic origin share the same characteristics. We analysed the Burkitt lymphoma cells BL41, compared with the same cells infected with Epstein Barr Virus (EBV), the E2r cell line [20]. Also in E2r EBV confers a high degree of resistance to apoptosis induced by a variety of stimuli (see below), thus partly accounting for EBV role in tumour progression [20]. A striking difference between these two cell lines, is the apoptotic morphology (achieved with apoptogenic agents such as puromycin or valinomycin), that is predominantly cleavage in the parental BL41, and predominantly budding in the converted E2r (Fig. 6A and B). We decided to exploit this separated distribution of the two morphologies to probe the correlation between apoptotic GSH loss and type of nuclear morphology. Thus, we performed a flow cytometric analysis of BL41 and E2r induced to apoptosis by PMC, stained with OPTA as GSH probe. Fig. 7A shows that in BL41 treated with PMC an extra peak at lower OPTA fluorescence appears, whose quantification coincides with the extent of apoptosis measured as the fraction of altered nuclei (Fig. 7A, bottom). Instead, in the E2r cells induced to apoptosis no extra peak is detectable (Fig. 7A), despite the fact that apoptosis normally took place (Fig. 7A, bottom). To confirm this result at the single cell level, we performed a quantitative image analysis of BL41 and E2r induced to apoptosis by PMC, and doubly stained, with Hoechst 33342 to detect nuclear morphology, and CMFDA for GSH quantisation. The results, shown in Fig. 7B, demonstrate a close correlation between type of nuclear apoptotic morphology and GSH content.

The differential behaviour and role of GSH in apoptosis in the two cell lines, were confirmed by inhibiting GSH efflux with cystathionine or methionine: this treatment reduced apoptosis in BL41 whereas E2r were insensitive (Fig. 8).

4. Discussion

Morphological alterations in apoptosis are a very dramatic phenomenon, with cells that lose their regular shape to suddenly acquire different features [26]. Such features may vary from cell to cell, or even in the same group of cells, being nonetheless very much reproducible and suggestive of an orchestrated set of events. This organisation reflects the very organised set of events that is known to characterise apoptosis from the molecular and biochemical point of view. Even though it is quite obvious that morphological alterations are the consequence of specific biochemical and molecular reactions, the use of morphological markers to label different biochemical events occurring in apoptosis, has not been fully explored (and exploited) so far.

Here we show that, in a set of cells of haematopoietic origin, two easily discernible morphological features of apoptosis such as nuclear vesiculation by cleavage or budding are linked to, and depend from, the extrusion/lack of

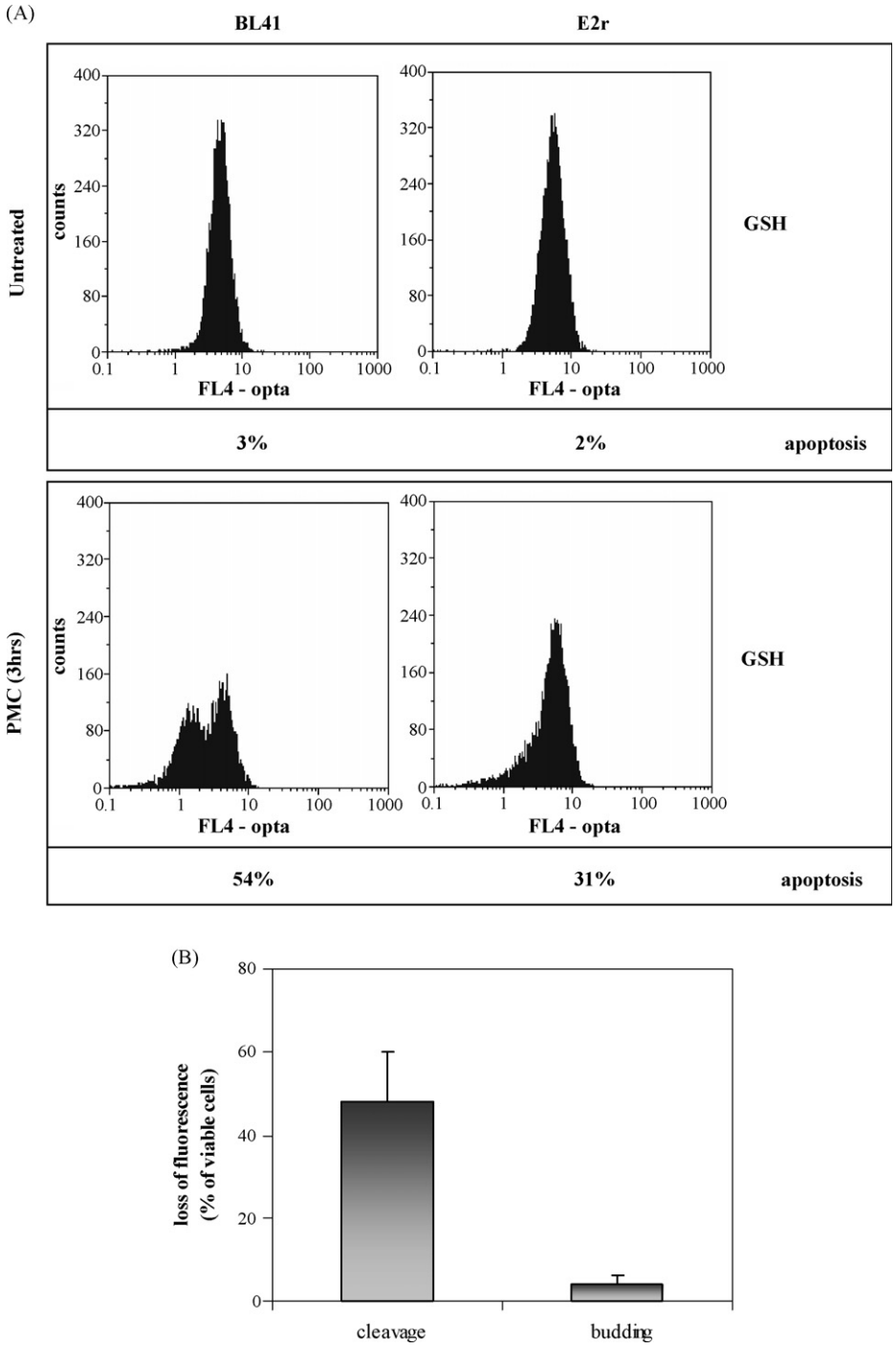

Fig. 7 – The correlation between GSH content and type of apoptotic morphology is maintained also in the BL41/E2r systems. The flow cytometric profile of BL41 (left column) and E2r (right column) cells stained with OPTA for GSH detection and pushed to apoptosis with PMC is shown in panel A. The corresponding extent of apoptosis is given below each profile. BL41 develop a low fluorescence peak upon apoptosis, whose quantisation corresponds to the extent of apoptosis. Instead, E2r do not show such extra peak in spite of apoptosis. The results were confirmed by additional experiments with similar results ($n = 2$). In panel B, a direct quantisation of the CMFDA fluorescence of apoptotic cells in cleavage or budding was performed by image analysis of Hoechst stained cells as described in Section 2, and compared with that of viable cells. The results are given as the loss of CMFDA fluorescence with respect to control cells, calculated in 100 E2r and BL41 cells.

extrusion of GSH as an early step of the apoptotic signalling. A similar relation between apoptotic nuclear morphology and intracellular GSH levels in apoptosis was found in two independent primary glioblastoma cell lines, which undergo apoptosis by two different morphological routes, leading to two different nuclear morphology, namely nuclear vesiculation and nuclear shrinkage: these two morphologies are accompanied by a different fate of their GSH, which is lost in

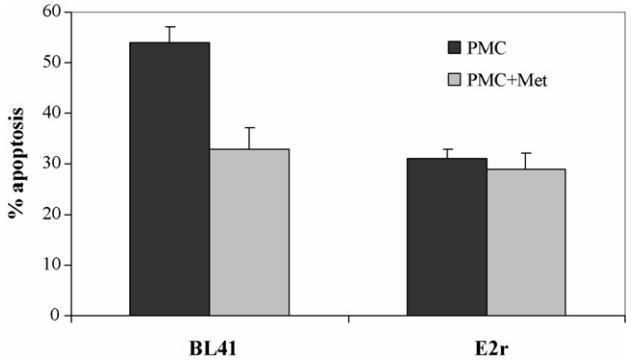

Fig. 8 – Effect of inhibition of GSH efflux on apoptosis of lymphoma cells. The extent of apoptosis was evaluated and quantified as described in Section 2 at 3 h of treatments with PMC, in the presence/absence of the inhibitor of GSH efflux methionine (met). Values are calculated as the average ± S.D. (n = 5). Methionine by itself does not exert any apoptogenic effect (not shown). The inhibition of GSH efflux reduces apoptosis on BL41 whereas it does not exert any anti-apoptotic effect on E2r. Similar results were obtained with cystathionine (not shown).

the vesiculating, but maintained in the shrunken, cells (Clavarino, ''tesi di laurea'').

The couple of lymphoma cell lines separately showing the two nuclear morphologies indicates that the infection with EBV, whose genome persists in the cells expressing the latent genes, provide E2r cells with the ability of contrasting the cleavage route. It is interesting to note that E2r are much less prone to apoptosis with respect to the parental BL41 [20], and the inhibition of cleavage may account, at least in part, for such resistance. Interestingly, different apoptotic morphologies in lymphomas were previously attributed to EBV latent infection [27]. The finding that the two apoptotic morphologies we describe depend on different redox status suggests that, in biochemical terms, the role of EBV in determining a shift in apoptotic morphology may depend on the different redox balance of the BL41 EBV-cells versus the EBV converted E2r, since it was demonstrated that EBV latent infection increase the oxidative status of the cells [20].

The notion that redox alterations induced by GSH efflux cause apoptosing cells to undertake the cleavage morphological route means that one or more of the actors of intracellular apoptotic signalling are redox modulated. This implies that a parallel redox signalling may overlap the canonical apoptotic pathways, resulting in different final features. A likely target of such redox signaling is the actin cytoskeleton, which is very sensitive to redox modulation [17]: the striking morphological alterations of apoptosis known as plasma membrane blebbing, due to deep actin remodelling [28], depend on redox alterations [29]. We have shown that cleavage requires a deep reshaping of the actin cytoskeleton and is strictly associated to blebbing, whereas the budding nuclear morphology develops exclusively in the absence of plasma membrane blebbing (De Nicola et al., submitted). The finding that the usually cytosolic actin may play a role in determining nuclear apoptotic morphology is supported by recent findings demonstrating that apoptogenic stimuli promote the formation of actin fibers in the nucleus [30]. For these reasons we hypothesize that the very rapid GSH loss occurring in apoptosis may alter intracellular redox equilibrium to such an extent as to remodel the actin cytoskeleton and to shift the nuclear morphology towards cleavage.

Caspases might also respond to redox alterations [13] due to reactivity of the cysteine residue in the active site, thus being possible mediators of the redox signalling promoting cleavage. Especially interesting is the finding that caspase 8, the initiator caspase of the extrinsic pathway, requires GSH in order to work [31]. We have shown that the extrinsic apoptotic pathway, induced through stimulation of physiological receptors (i.e., Fas) may occur without redox alterations and may be achieved independently of Bax translocation or cytochrome c release [11]. Instead, the intrinsic pathway, which is primed by caspase 9 instead of caspase 8, requires redox modulation, Bax translocation and cytochrome c release [7]. We have also shown that the apoptotic GSH extrusion occurs only in the intrinsic apoptotic pathway (De Nicola, in preparation). Thus, the correlation between the intrinsic apoptotic pathway and GSH efflux in apoptosis on the one side, and between the extrinsic pathway and GSH retention on the other, tempts us to speculate that budding might be the result of physiological apoptosis, whereas cleavage might be the result of stress-induced apoptosis. Further studies are on the way in our laboratory to analyse whether a different pattern of caspase activation is activated in cells undergoing apoptosis along the budding versus the cleavage route.

An obvious question is what determines the choice between budding and cleavage in apoptosing U937. Our data indicate that if and once GSH is extruded, the cleavage route begins; now the question becomes what determines the decision of an apoptosing cells as to whether extruding or retaining GSH. Apoptotic GSH extrusion occurs in U937 through the synusoidal GSH carriers [9] used by several cell types for physiologically exporting GSH into the extracellular fluids [32,33]; in apoptosis the GSH efflux rate is strongly increased and accelerated [8]. This means that carriers may be activated during apoptosis, but the mechanism is still obscure. Indeed, GSH transport occurs passively in a gradient-dependent fashion, and no physiological regulation mechanisms have been described so far. We have evidences that caspase 2, whose role in apoptosis is still controversial, may possibly determine GSH carriers activation (De Nicola, in preparation). This could account for the suggested role of caspase 2 as a very upstream activator of the intrinsic apoptotic pathway [34].

The finding that in U937 budding and cleavage co-exist might be explained by hypothesizing either genetic heterogeneity (often developing in continuous culture of tumour cells), implying that a set of cells are destined to one or the other route. Alternatively, each cell has the potentiality of undergoing one or the other pathway, the decision being of a stochastic nature. We are tempted to exclude the first explanation, for the following reasons. If we extend the analysis of apoptosis induced in the presence of cystathionine or methionine for longer times, all cells develop apoptosis via the budding route (not shown); moreover, inhibitors of mono-(ADP-ribosylation) reactions completely shift

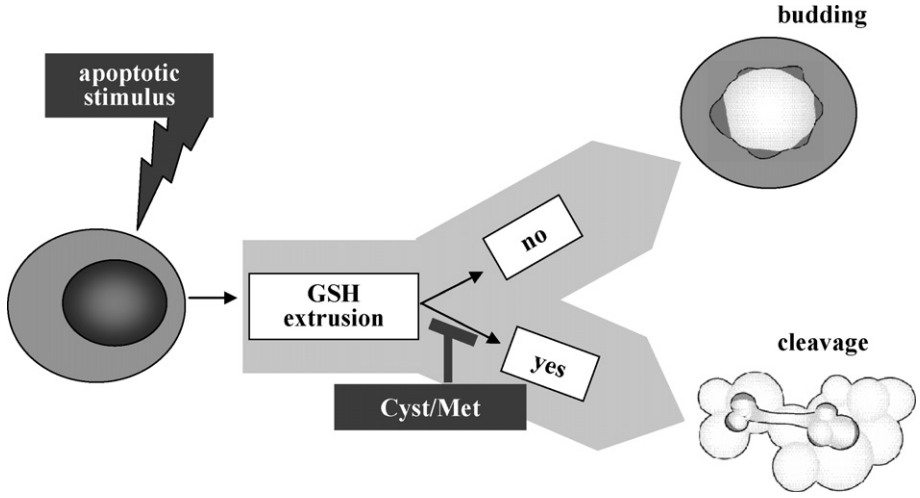

Fig. 9 – Different fates of intracellular glutathione determine different apoptotic morphologies. In U937, BL41 and E2r cells intracellular GSH is lost in cells undergoing apoptosis by cleavage, whereas it is maintained in apoptotic budding cells. GSH depletion is the determinant of the cleavage route, since the inhibition of apoptotic GSH efflux with cystathionine or methionine shifts the apoptotic morphology from cleavage to budding.

damage-induced apoptosis to the cleavage route [35]. This indicate that all possess the potentiality of undergoing both routes, and that the two routes may be differently affected by different metabolic inhibitors.

The results shown in the present study propose a novel marker that, by morphological criteria, might help to individuate cells that may respond or not to different type of chemosensitisation. The findings described in this study, summarized in Fig. 9, are a first step in a task we are performing, that is trying to connect biochemical and morphological alterations, with the implication that the latter are the result of the former.

REFERENCES

[1] Gupta S. Molecular steps of death receptor and mitochondrial pathways of apoptosis. Life Sci 2001;69: 2957–64.
[2] Kischkel FC, Hellbardt S, Behrmann I, Germer M, Pawlita M, Krammer PH, et al. Cytotoxicity-dependent APO-1 (Fas/CD95)-associated proteins form a death-inducing signaling complex (DISC) with the receptor. EMBO J 1995;14(22):5579–88.
[3] Peter ME, Krammer PH. Mechanisms of CD95 (APO-1/Fas)-mediated apoptosis. Curr Opin Immunol 1998;10:545–51.
[4] Zou H, Li Y, Liu X, Wang X. An APAF-1.cytochrome c multimeric complex is a functional apoptosome that activates procaspase-9. J Biol Chem 1999;274:11549–56.
[5] Kluck RM, Bossy-Wetzel E, Green DR, Newmeyer DD. The release of cytochrome c from mitochondria: a primary site for Bcl-2 regulation of apoptosis. Science 1997;275:1132–6.
[6] Jiang X, Wang X. Cytochrome c promotes caspase-9 activation by inducing nucleotide binding to Apaf-1. J Biol Chem 2000;275:31199–203.
[7] Coppola S, Ghibelli L. GSH extrusion and the mitochondrial pathway of apoptotic signalling. Biochem Soc Trans 2000;28:56–61.
[8] Ghibelli L, Coppola S, Rotilio G, Lafavia E, Maresca V, Ciriolo MR. Non-oxidative loss of glutathione in apoptosis via GSH extrusion. Biochem Biophys Res Commun 1995(a);216:313–20.
[9] Ghibelli L, Fanelli C, Rotilio G, Lafavia E, Coppola S, Colussi C, et al. Rescue of cells from apoptosis by inhibition of active GSH extrusion. FASEB J 1998;12: 479–86.
[10] Van den Dobbelsteen D, Nobel S, Schlegel J, Cotgreave IA, Orrenius S, Slater A. GSH effflux in FAS/APO-1-induced apoptosis. J Biol Chem 1996;271:15420–7.
[11] D'Alessio M, De Nicola M, Coppola S, Gualandi G, Pugliese L, Cerella C, et al. Oxidative Bax dimerization promotes its translocation to mitochondria independently of apoptosis. FASEB J 2005;19(11):1504–6.
[12] Ghibelli L, Coppola S, Fanelli C, Rotilio G, Civitareale P, Scovassi AI, et al. Glutathione depletion causes cytochrome c release even in the absence of cell commitment to apoptosis. FASEB J 1999;13:2031–6.
[13] Hampton MB, Fadeel B, Orrenius S. Redox regulation of the caspases during apoptosis. Ann N Y Acad Sci 1998;854:328–35.
[14] Lind C, Gerdes R, Schuppe-Koistinen I, Cotgreave IA. Studies on the mechanism of oxidative modification of human glyceraldehyde-3-phosphate dehydrogenase by glutathione: catalysis by glutaredoxin. Biochem Biophys Res Commun 1998;247(2):481–6.
[15] Nakamura Y, Ohigashi H, Masuda S, Murakami A, Morimitsu Y, Kawamoto Y, et al. Redox regulation of glutathione S-transferase induction by benzyl isothiocyanate: correlation of enzyme induction with the formation of reactive oxygen intermediates. Cancer Res 2000;60(2):219–25.
[16] Arien H, Wiser O, Arkin IT, Leonov H, Atlas D. Syntaxin 1A modulates the voltage-gated L-type calcium channel (Ca(v)1,2) in a cooperative manner. J Biol Chem 2003;278(31):29231–9.
[17] Dalle-Donne IR, Rossi A, Milzani P, Di Simplicio P, Colombo R. The actin cytoskeleton response to oxidants: from small heat shock protein phosphorylation to changes in the redox state of actin itself. Free Radical Biol Med 2001;31:1624–32.

[18] Mirabelli F, Salis A, Marinoni V, Finardi G, Bellomo G, Thor H, et al. Menadione-induced bleb formation in hepatocytes is associated with the oxidation of thiol groups in actin. Arch Biochem Biophys 1988;264(1):261–9.
[19] Dini L, Coppola S, Ruzittu MT, Ghibelli L. Multiple pathways for apoptotic nuclear fragmentation. Exp Cell Res 1996;223:340–7.
[20] Gualandi G, Giselico L, Carloni M, Palitti F, Mosesso P, Alfonsi AM. Enhancement of genetic instability in human B cells by Epstein-Barr virus latent infection. Mutagenesis 2001;16:203–8.
[21] Ghibelli L, Maresca V, Coppola S, Gualandi G. Protease inhibitors block apoptosis at intermediate stages: a compared analysis of DNA fragmentation and apoptotic nuclear morphology. FEBS Lett 1995(b);377:9–14.
[22] Coates A, Tripp E. Comparison of two fluorochromes for flow cytometric assay of cellular glutathione content in human malignant melanoma. Melanoma Res 1995;5(2):107.
[23] Keelan J, Allen NJ, Antcliffe D, Pal S, Duchen MR. Quantitative imaging of glutathione in hippocampal neurons and glia in culture using monochlorobimane. J Neurosci Res 2001;66(5):873–84.
[24] Stevenson D, Wokosin D, Girkin J, Grant MH. Measurement of the intracellular distribution of reduced glutathione in cultured rat hepatocytes using monochlorobimane and confocal laser scanning microscopy. Toxicol In Vitro 2002;16(5):609–19.
[25] Treumer J, Valet G. Flow-cytometric determination of glutathione alterations in vital cells by o-phthaldialdehyde (OPT) staining. Exp Cell Res 1986;163(2):518–24.
[26] Rogalinska M. Alterations in cell nuclei during apoptosis. Cell Mol Biol Lett 2002;7:995–1018.
[27] Ishii H, Gobe GC, Joshita T, Kurabayashi Y, Hosomura Y, Kameya T. Analysis of apoptosis morphology in Epstein-Barr virus positive and negative Burkitt's lymphoma cells. Arch Histol Cytol 1997;60:143–52.
[28] Ghibelli L, Nosseri C, Coppola S, Maresca V, Dini L. The increase in H2O2-induced apoptosis by ADP-ribosylation inhibitors is related to cell blebbing. Exp Cell Res 1995;221(2):470–7.
[29] Jewell SA, Bellomo G, Thor H, Orrenius S, Smith M. Bleb formation in hepatocytes during drug metabolism is caused by disturbances in thiol and calcium ion homeostasis. Science 1982;217:1257–9.
[30] Luchetti F, Burattini S, Ferri P, Papa S, Falcieri E. Actin involvement in apoptotic chromatin changes of hemopoietic cells undergoing hyperthermia. Apoptosis 2002;7(2):143–52.
[31] Hentze H, Schmitz I, Latta M, Krueger A, Krammer PH, Wendel A. Glutathione dependence of caspase-8 activation at the death-inducing signaling complex. J Biol Chem 2002;277(7):5588–95.
[32] Lu SC, Kuhlenkamp J, Ge JL, Sun WM, Kaplowitz N. Specificity and directionality of thiol effects on sinusoidal glutathione transport in rat liver. Mol Pharmacol 1994;46:578–85.
[33] Meredith MJ, Cusick CL, Soltaninassab S, Sekhar KS, Lu S, Freeman ML. Expression of Bcl-2 increases intracellular glutathione by inhibiting methionine-dependent GSH efflux. Biochem Biophys Res Commun 1998;248:458–63.
[34] Fumarola C, Guidotti GG. Stress-induced apoptosis: toward a symmetry with receptor-mediated cell death. Apoptosis 2004;9(1):77–82.
[35] Cerella C, D'Alessio M, De Nicola M, Magrini A, Bergamaschi A, Ghibelli L. Cytosolic and endoplasmic reticulum Ca2+ concentrations determine the extent and the morphological type of apoptosis, respectively. Ann N Y Acad Sci 2003;1010:74–7.